Journal of Molecular Catalysis A: Chemical 301 (2009) 24–30

Contents lists available at ScienceDirect

Journal of Molecular Catalysis A: Chemical

journal homepage: www.elsevier.com/locate/molcata

Characterization and catalytic application of highly dispersed manganese oxides supported on activated carbon

Qinghu Tang[a,b], Xiaona Huang[b], Yuanting Chen[a], Tao Liu[c], Yanhui Yang[a,*]

[a] School of Chemical and Biomedical Engineering, Nanyang Technological University, 62 Nanyang Drive, N1.2-B1-18, Singapore 637459, Singapore
[b] Department of Chemistry, Henan Normal University, Xinxiang 453007, China
[c] Singapore Synchrotron Light Source, National University of Singapore, 5 Research Link, Singapore 117603, Singapore

ARTICLE INFO

Article history:
Received 7 May 2008
Received in revised form 30 October 2008
Accepted 4 November 2008
Available online 13 November 2008

Keywords:
Manganese oxide
Activated carbon
Benzyl alcohol oxidation

ABSTRACT

Activated carbon supported manganese oxides (Mn/AC) were prepared by a conventional wet impregnation method using manganese nitrate as the precursor. The nature of supported manganese oxides, e.g., dispersion, oxidation state, local coordination, was characterized by X-ray diffraction (XRD), electron spin resonance (ESR), X-ray absorption near edge structure (XANES), extended X-ray absorption fine structure (EXAFS) spectroscopies, and hydrogen temperature-programmed reduction (H_2-TPR). Manganese loading and pretreatment temperature were found to be vital factors in controlling the dispersion and chemical environment of supported manganese oxides. Highly dispersed manganese oxides can be obtained with a Mn loading up to ca. 5 wt.% under modest pretreatment temperatures, whereas large amount of Mn resulted in aggregated MnO_x crystalline clusters. The highly dispersed manganese oxides, uniformly distributed on activated carbon surface mainly as coexistence of Mn^{2+} and Mn^{3+}, have been demonstrated to be catalytically active in the aerobic oxidation of benzyl alcohol using molecular oxygen. Benzyl alcohol conversion as high as 42.5% and over 99% benzaldehyde selectivity can be achieved within 4 h under low reaction temperature (373 K).

1. Introduction

Both supported and unsupported manganese oxides have received great attention as catalytically active components in a variety of catalytic reactions, e.g., the decomposition of ozone [1,2], N_2O [3,4], and 2-propanol [5]; the oxidation of carbon monoxide [6–8], alcohol [9–13], ethylene [14], benzene [15], ammonia [16], and hydrocarbon [7,17]; the hydrogenation of ethylene [9]; the removal of hydrogen sulfide [18]; and the low-temperature selective catalytic reduction of NO with NH_3 [19–22]. Moreover, manganese oxides have been employed for the catalytic combustion of volatile organic compounds [23].

Carbonaceous materials are promising catalyst supports because of their low cost and lack of prospective problems concerning removal after deactivation. Activated carbon (AC) supported catalysts hold several advantages comparing with silica- and alumina-supported catalysts. Interaction between support and active component is minimized to a large extent due to the inert graphitic surface, which leads to an optimized utilization of active sites [24,25]. The thermal stability of activated carbon at elevated temperature is remarkably higher than that of SiO_2 and Al_2O_3 in inert environments [26]. Another important reason using activated carbon as support is due to its high stability in caustic and acidic conditions. In comparison to other catalytically inert supports, carbonaceous materials do not only play a role as catalyst support, high activity is also registered for the carbon materials in many cases, partially due to the enriched surface oxygen complexes [27–29].

Although there are numerous reports dealing with manganese supported on carbon materials [19,21,22,30–35], some ambiguities about the nature of catalytically active manganese sites on activated carbon still remain unsolved, especially when manganese oxide species are highly dispersed on the support. It is not clear whether the manganese oxide presents in the form of single oxidation state or a mixture of oxidic phases. The local coordination of manganese has not been undoubtedly elucidated as well. It is also desired to understand whether the Mn species exist as isolated species or two-dimensional clusters on the activated carbon surface. As the above-mentioned issues are extremely important for the explanation of manganese chemistry, there is an impetus to have a thorough characterization of manganese over activated carbon support.

The present work is aimed to characterize the nature of Mn species formed on activated carbon. Manganese loading and pretreatment temperature, two crucial factors controlling the dispersion and local environment of manganese oxides, will be discussed in detail. Various characterization techniques such as

* Corresponding author. Tel.: +65 6316 8940; fax: +65 6794 7553.
E-mail address: yhyang@ntu.edu.sg (Y. Yang).

1381-1169/$ – see front matter © 2008 Elsevier B.V. All rights reserved.
doi:10.1016/j.molcata.2008.11.003

nitrogen physisorption, X-ray diffraction (XRD), electron spin resonance (ESR), X-ray absorption near edge structure (XANES), extended X-ray absorption fine structure (EXAFS) spectroscopies, and hydrogen temperature-programmed reduction (H_2-TPR) will be employed to describe the physicochemical properties of Mn species used for the aerobic oxidation of benzyl alcohol with molecular oxygen. In addition, the reactivity of Mn catalysts will be evaluated, with emphasis on the correlation with surface manganese species and pretreatment conditions.

2. Experimental

2.1. Catalyst preparation

High purity activated carbon (Scharlau Chemie) was pretreated using HNO_3 (1 M) and deionized water. After washing and drying, the Brunauer–Emmett–Teller (BET) specific surface area was 856 $m^2\,g^{-1}$, total ash content was below 0.1 wt.%. Manganese oxide was deposited on activated carbon using aqueous solutions of manganese nitrate by a conventional wet impregnation method. In a typical preparation, 20 ml of deionized water was added to a beaker containing 2.0 g of activated carbon. A measured amount of manganese nitrate precursor was added to the above-mentioned solution under vigorous stirring. The mixture was further stirred for 3 h, and allowed to rest for 24 h under ambient condition. The Mn impregnated activated carbon powder was obtained by heating at 343 K to evaporate water, followed by drying in vacuum at 313 K overnight and incubating in a helium flow of 40 ml min^{-1} at 673 K for 6 h.

2.2. Characterization

Nitrogen physisorption was measured at 77 K with a static volumetric Autosorb 6B (Quanta Chrome). Prior to measurement, the samples were outgassed at 473 K to a residual pressure below 10^{-4} Torr. A Baratron pressure transducer (0.001–10 Torr) was used for low-pressure measurements. The specific surface area was calculated by the standard Brunauer–Emmett–Teller method. Powder X-ray diffraction patterns were recorded using a Bruker Advance 8 X-ray diffractometer equipped with a rotating anode using Cu Kα radiation ($\lambda = 0.154$ nm), operating at 40 kV and 40 mA. ESR spectra were measured using a Bruker EMX ESR spectrometer at X-band (~9 GHz). The powder sample was loaded into a quartz tube with inner diameter of 3 mm and measured under ambient condition.

X-ray absorption measurements at Mn K-edge were performed at the X-ray demonstration and development beam line of the Singapore Synchrotron Light Source (SSLS) where a Si(1 1 1) channel-cut monochrometer is equipped [36]. The samples were ground into fine powders, pressed into self-supporting wafers, placed in a stainless steel cell, and measured in transmission mode from 6450 eV to 7450 eV at room temperature. The electron energy in the storage ring was about 700 MeV with a current of about 200 mA. Incident and transmitted X-ray intensities were measured by two ionization chambers filled with pure nitrogen. Energy was calibrated using Mn foil (6539.0 eV). The spectra collected were analyzed using the WinXAS 2.3 code. The theoretical EXAFS functions for different Mn species (MnO_2 and Mn_3O_4) generated by the FEFF6 were used to fit the experimental data in order to calculate the Mn–Mn and Mn–O and coordination numbers (CNs) [37].

The reducibility and the stability of Mn supported on activated carbon samples were investigated by a temperature-programmed reduction technique using Autosorb-1C equipped with a thermal conductivity detector (TCD). Prior to each H_2-TPR run, the sample (approximately 100 mg) was purged by ultra zero grade air at room temperature, then the temperature was increased to 573 K at 5 K min^{-1}, soaked for 1 h at the same temperature, and cooled down to room temperature. This procedure produced a clean surface before running the H_2-TPR. The gas flow was switched to 5 vol.% hydrogen in argon balance, and the base line was monitored until stable. After baseline stabilization, the sample cell was heated at 5 K min^{-1} rate and held for 1 h at 1173 K to ensure complete manganese reduction.

2.3. Catalytic reaction

The catalytic oxidation of benzyl alcohol with molecular O_2, carried out using a bath-type reactor operated under atmospheric condition, was used as a probe reaction to investigate the oxidation state and dispersion of the supported manganese species. In a typical reaction run, a certain amount of catalyst was loaded to a glass flask pre-charged with 2 mmol benzyl alcohol and 10 ml toluene, the mixture was then heated to the reaction temperature (373 K) under vigorous magnetic stirring (800 rpm). Oxygen flow was bubbled at a flow rate of 10.0 ml min^{-1} into the mixture to start the reaction once the reaction temperature is reached. Dodecane was used as the internal standard. After reaction, the solid catalyst was filtered off and the liquid organic products were analyzed by an Agilent gas chromatograph (GC) 6890 equipped with a HP-5 capillary column (30 m long and 0.32 mm in diameter, packed with silica-based supel cosil). Calibration of GC peak areas was carried out using solutions with known amounts of benzyl alcohol, benzaldehyde, benzoic acid, and benzyl benzoate in toluene. The conversion was calculated in the basis of molar percentage of benzyl alcohol. The initial molar percentage of benzyl alcohol was divided by initial area percentage to get the response factor. The amount of unreacted alcohol in the reaction mixture was calculated by multiplying the GC peak area percentage of benzyl alcohol obtained after reaction with the response factor. The conversion, selectivity, and turnover number (TON) were calculated as follows:

$$\text{conversion (mol\%)} = \frac{\text{initial mol\%} - \text{final mol\%}}{\text{initial mol\%}}\ 100\% \quad (1)$$

$$\text{aldehyde selectivity (\%)} = \frac{\text{GC peak area of aldehyde}}{\text{GC peak area of all products}}\ 100\% \quad (2)$$

$$\text{TON} = \frac{\text{number of moles of aldehyde formed}}{\text{number of moles of manganese in the catalyst}} \quad (3)$$

3. Results and discussion

3.1. XRD results

X-ray diffraction is one of the most important techniques for characterizing the structural conformation of crystalline materials. Fig. 1 shows the XRD patterns of Mn/AC samples with different manganese contents. Only diffractions ascribed to activated carbon appear when the Mn loading is lower than ca. 5 wt.%; no crystalline manganese oxide peak can be observed. Weak diffraction peaks at 2θ of 18.1°, 28.9°, 32.4°, 36.2°, 44.3°, 58.5° and 59.8° assignable to crystalline Mn_3O_4 become noticeable when the Mn content is more than ca. 10 wt.%. These results suggest that manganese oxides are highly dispersed over activated carbon with the Mn loading amount lower than ca. 5 wt.%, forming MnO_x nano-clusters with diameter below the detect limit of XRD; whereas aggregation of large Mn_3O_4 clusters occurs when excess amount of manganese is in presence. We also note a weak diffraction peak assignable to crystalline MnO at 2θ of 40.6° in 20 wt.% Mn/AC, which is probably due to the partial

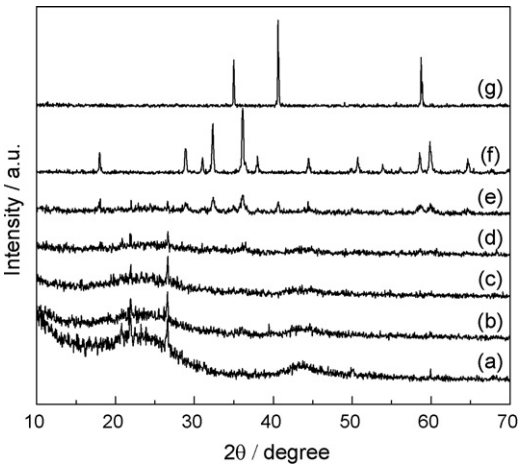

Fig. 1. X-ray diffraction patterns of the Mn/AC catalysts as well as Mn_3O_4: (a) activated carbon; (b) 3 wt.% Mn/AC; (c) 5 wt.% Mn/AC; (d) 10 wt.% Mn/AC; (e) 20 wt.% Mn/AC; (f) Mn_3O_4; (g) MnO.

decomposition of manganese nitrate precursor at high loading in this particular sample.

3.2. ESR results

ESR spectroscopy monitors paramagnetic isolated species and gives information about the oxidation state and local coordination structure of isolated metal site. Consequently, it can be used to characterize Mn^{2+} and Mn^{4+} species with high dispersion on the support, whereas Mn^{3+} species usually cannot be detected due to the complete splitting of energy levels (no ground-state degeneracy) [38,39]. The ESR spectra of Mn/AC samples measured at room temperature are depicted in Fig. 2. The 3 wt.% and 5 wt.% Mn/AC samples show a broad Lorentzian-shape signal with $g = 2.04$ and a poorly resolved six-line hyperfine structure with average splitting constant $A = 91.04$ G, which are consistent with Mn^{2+} ($g = 2.0$, $A = 80–100$ G) in the environment of distorted octahedral symmetry [40,41]. Increasing the Mn content (5 wt.%) slightly broadens the hyperfine structure and results in a decrease in the spectrum resolution. This may be attributed to an increase in the spin exchange interaction due to the decrease of Mn^{2+}–Mn^{2+} distance [25,42]. As for the 5 wt.% Mn/AC sample treated at 873 K, the hyperfine curve significantly broadens, which can be explained by the dipole–dipole interactions between magnetic ions in a magnetically concentrated system [43]. This remarkable change suggests that a high pretreatment temperature may induce a major change in the nature of Mn species on activated carbon although how the change occurred remains unclear due to the low resolution of ESR spectra in this study.

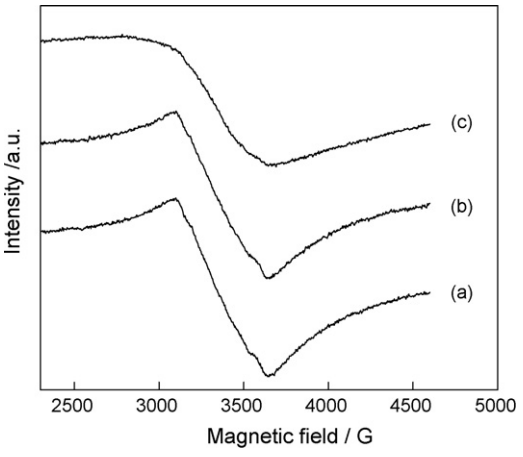

Fig. 2. ESR spectra of (a) 3 wt.% Mn/AC-673 K, (b) 5 wt.% Mn/AC-673 K, and (c) 5 wt.% Mn/AC-873 K.

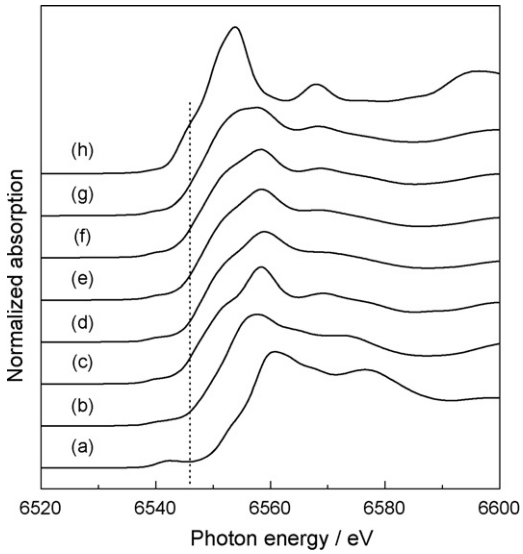

Fig. 3. Mn K-edge XANES spectra: (a) MnO_2; (b) Mn_2O_3; (c) Mn_3O_4; (d) 3 wt.% Mn/AC-673 K; (e) 5 wt.% Mn/AC-673 K; (f) 20 wt.% Mn/AC-673 K; (g) 5 wt.% Mn/AC-873 K; (h) MnO.

3.3. X-ray absorption results

X-ray absorption spectroscopy (XAS) with synchrotron light source has emerged as a powerful technique to probe the active site in catalysis [44–46]. X-ray absorption near edge structure and extended X-ray absorption fine structure provide information about the local coordination and electronic properties of the catalyst active centers [1,41,47]. Manganese oxides supported on Al_2O_3, ZrO_2, TiO_2, and SiO_2 have been extensively studied using X-ray absorption techniques [48–50]. In this study, XAS was used to compliment ESR spectra to characterize more detailed insight into the oxidation state and local coordination structure of manganese oxides supported on carbon. The normalized XANES spectra at the Mn K-edge of the Mn/AC samples as well as the reference manganese oxides are illustrated in Fig. 3. Various Mn species exhibit well-defined, distinct XANES features. The small pre-edge peaks in XANES are attributed to the 1*s*-3*d* transition. All Mn/AC samples treated at 673 K show almost identical pre-edge features, indicating the similar valence of manganese ion species in these samples, regardless of Mn content. X-ray absorption main edge positions and the average valences are shown in Table 1. The average valence of Mn in 3 wt.% and 5 wt.% Mn/AC samples are 2.69 and 2.67, respectively, which are close to that of Mn_3O_4 (2.67), implying the

Table 1
X-ray absorption-main edge position and the average valence.

Sample	Edge position/eV[a]	Valence
3 wt.% Mn/AC-673 K	6546.8	2.69
5 wt.% Mn/AC-673 K	6546.7	2.67
5 wt.% Mn/AC-873 K	6545.9	2.46
20 wt.% Mn/AC-673 K	6546.5	2.62
MnO	6544.0	2.00
Mn_3O_4	6546.5	2.67
Mn_2O_3	6548.5	3.00
MnO_2	6551.9	4.00

[a] Taken as the first major maximum in the derivative of the K-edge spectrum with respect to the corresponding feature of Mn foil (6539.0 eV).

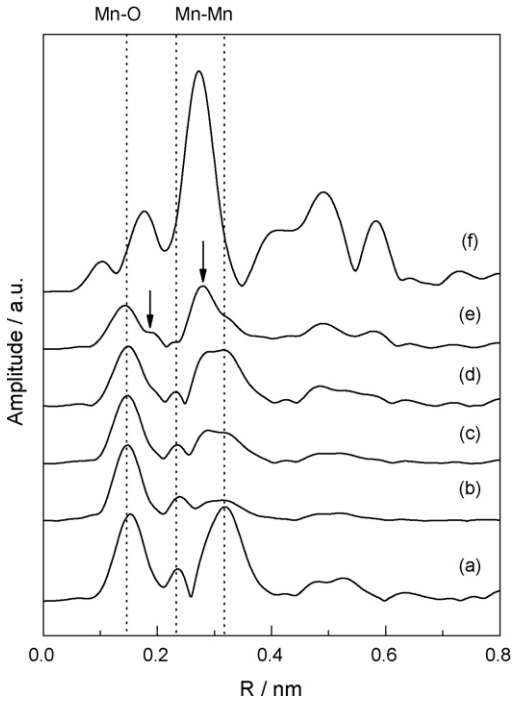

Fig. 4. Fourier transforms of the Mn K-edge EXAFS spectra (phase shift was not corrected): (a) Mn_3O_4; (b) 3 wt.% Mn/AC-673 K; (c) 5 wt.% Mn/AC-673 K; (d) 20 wt.% Mn/AC-673 K; (e) 5 wt.% Mn/AC-873 K; (f) MnO.

coexistence of Mn^{2+} and Mn^{3+}. According to the results reported by Yang et al. [51], Mn_3O_4 has a normal spinel structure with Mn^{2+} ions in tetrahedral sites and Mn^{3+} ions in tetragonally-distorted octahedral sites. In view of our ESR and XANES characterizations, it may be reasonable to assume that the Mn^{2+} species on carbon surface occupy a distorted octahedral and/or distorted tetrahedral coordination, whereas the Mn^{3+} species locate in the octahedral coordination sites [40]. Slightly lower average Mn valance for 20 wt.% Mn/AC sample (2.62) than that of Mn_3O_4 may arouse from small amount of MnO in this particular sample as suggested by XRD. The Mn/AC sample treated at 873 K (5 wt.% Mn/AC-873 K) shows an average Mn valence of 2.46, suggesting the appearance of more Mn^{2+} ions in this sample.

At the time that EXAFS was introduced in catalysis around 1975, the technique was considered to be one of the most promising tools for investigating catalysts. It gives detailed local conformational information, such as the coordination number, bond length, etc. Fig. 4 shows the Fourier transforms of the k^3 weighted EXAFS data for Mn/AC samples as well as Mn_3O_4 and MnO reference (phase shift was not corrected). The Mn_3O_4 reference spectrum shows two strong peaks at 0.15 nm and 0.30 nm, which can be assigned to Mn–O coordination on the first shell and the second shell which contains a mixture of Mn–O and Mn–Mn coordination. The weak feature at 0.24 nm is due to the Mn–Mn coordination. For activated carbon supported samples treated at 673 K, mainly one strong peak at 0.15 nm and two weak peaks at 0.24 nm and 0.30 nm are depicted, indicating a similar local coordination compared to that of Mn_3O_4. The fitting was carried out for Mn–O and Mn–Mn coordinations in *k*-space by filtering out respective peaks in Fourier transform from *R*-space to *k*-space. The structural parameters obtained are summarized in Table 2. For crystalline Mn_3O_4, it is of distorted spinal structure with a tetragonal lattice containing two non-equivalent Mn sites, tetrahedral and octahedral as reported elsewhere [52]. The octahedral Mn sites have four Mn–O bonds of length 0.1932 nm, two Mn–O bonds of length 0.2284 nm, and two Mn–Mn bonds of length 0.2884 nm, while the tetrahedral Mn site has four Mn–O bonds of length 0.2044 nm. In this study, only the average coordination number and bond length of Mn-ligand structure were given. For crystalline Mn_3O_4, the average CN for the first Mn–O shell is 5.1 (average of tetrahedral and octahedral Mn–O coordination), the average CN for Mn–Mn at 0.24 nm and 0.30 nm are 0.8 and 9.1, respectively. These coordination numbers are in good agreement with the crystallographic data reported elsewhere [53], confirming the validity of spectra analyses in this study. Furthermore, the EXAFS data were recorded up to $k = 16\ Å^{-1}$ (not shown here) in *k*-space, which allows a more sophisticate multi-parameter data fit. Compare to crystalline Mn_3O_4, the manganese species supported on activated carbon show a smaller CN for Mn–O at 0.15 nm and smaller CN for Mn–Mn at 0.24 nm, implying more tetrahedral Mn sites than that of bulk Mn_3O_4. This is probably due to the highly dispersive Mn species in the carbon matrix, some Mn–O bonds are not saturated at carbon surface. At lower Mn loading, e.g., ca. 3 wt.%, the second Mn–Mn shell coordination number is 2.3, indicating manganese oxide species are highly dispersed on the surface of activated carbon. A slight increase in CN for the Mn–Mn coordination at 0.30 nm is noted with the increase of the Mn loading amount (5 wt.%). A high Mn loading (ca. 20 wt.%) results in a Mn–Mn CN of 6.8, suggesting larger crystalline domain size. These results further support the XRD characterization. Compare to the corresponding sample treated at 673 K, significant changes can be discerned in the Fourier transform spectra of 5 wt.% Mn/AC-873 K (Fig. 4). With a high pretreatment temperature, the peak assigned to Mn–O becomes asymmetric and a shoulder peak at high *R*-value (0.18 nm) appears, and the second peak assigned to Mn–Mn coordination on the second shell shifts to 0.27 nm. Moreover, the weak feature at 0.24 nm due to the Mn–Mn coordination diminishes. Coincidently, MnO reference spectrum shows two strong peaks at 0.18 nm and 0.27 nm, which can be assigned to Mn–O coordination on the first shell and Mn–Mn coordination on the second shell, respectively. It is suggested a conversion from Mn^{3+} to Mn^{2+} in the octahedral coordination sphere occurs under a high pretreatment temperature.

3.4. H_2-TPR results

Reducibility of the Mn species has been related to the catalytic activity of manganese catalysts. Hydrogen temperature-programmed reduction is a convenient technique for studying the reduction behavior of supported oxide catalysts qualitatively. In this study, H_2-TPR is carried out in the temperature range from 323 K to 1173 K for the purpose of investigating the reduction behavior of the manganese species as a stability index. The H_2-TPR patterns

Table 2
Results of EXAFS curve-fitting for M–O and Mn–Mn shells of Mn/AC sample series.[a].

Samples	CN (±10%)	*R*/nm (±0.001 nm)	$\Delta\sigma^2/\times10^{-5}$ nm^2 (±10%)	ΔE_0/eV (±10%)
Mn_3O_4	5.1	0.195	0.8	9.5
	0.8	0.275	0.4	−11.3
	9.1	0.350	0.8	15.3
3 wt.% Mn/AC-673 K	4.3	0.191	0.8	7.6
	0.6	0.283	0.4	−3.0
	2.3	0.344	0.8	4.6
5 wt.% Mn/AC-673 K	4.0	0.192	0.8	6.2
	0.4	0.277	0.4	−9.9
	3.5	0.344	0.8	3.3
20 wt.% Mn/AC-673 K	3.5	0.193	0.8	7.0
	0.4	0.276	0.3	9.2
	6.8	0.347	1.0	6.6

[a] CN, *R* and $\Delta\sigma^2$ are coordination number, bond length and Debye–Waller factor, respectively.

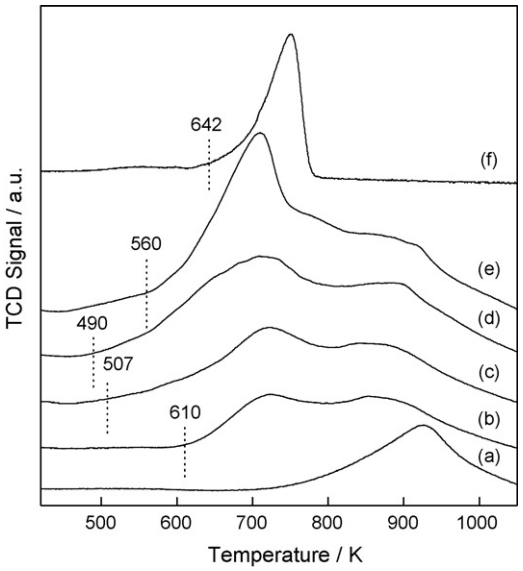

Fig. 5. H_2-TPR spectra for Mn/AC samples treated at 673 K: (a) activated carbon; (b) 3 wt.% Mn/AC; (c) 5 wt.% Mn/AC; (d) 10 wt.% Mn/AC; (e) 20 wt.% Mn/AC; (f) Mn_3O_4.

of Mn/AC samples treated at 673 K as well as reference compound Mn_3O_4 are shown in Fig. 5. The H_2-TPR profile of the activated carbon support (Fig. 5a) presents a broad reduction peak at 923 K which can be attributed to the oxygen complexes on carbon surface [54,55]. For the crystalline Mn_3O_4, only one sharp reduction peak is observed at 753 K, which is generally suggested as the reduction of Mn_3O_4 to MnO [20]. H_2-TPR patterns for all Mn/AC samples show two broad reduction peaks, centered at 723 K and 873 K. The first peak (723 K) can be assigned the reduction of manganese oxide species supported on activated carbon; the broad feature is probably related to the interaction between Mn and activated carbon support with a quite heterogeneous nature. The second peak (873 K) is suggested to be the reduction of the carbon support, the 50 K temperature shift (from 923 K to 873 K) can be explained by either interaction between carbon matrix of the support with Mn species, or different reduction kinetics followed by Mn oxide particles residing in different domain of the activated carbon. Similar results have been reported on the activated carbon supported Mo and Ni catalysts by Calafat et al. [56]. For the 3 wt.% Mn/AC sample, the reduction of manganese oxide species starts at a temperature as low as 610 K. A shift of onset reduction to low temperature with increasing Mn loadings is observed when the Mn content is lower than ca. 10 wt.%, suggesting more small manganese oxide clusters, weakly interacted with carbon support, are formed with the increase of Mn loadings. However, a remarkable increase of the onset reduction temperature is observable when the Mn loading is higher than ca. 10 wt.%. Such an increase may be related to the appearance of large aggregated manganese oxide clusters because the onset reduction of crystalline Mn_3O_4 generally occurs at a high temperature. These results agree well with the conclusion of XRD, XPS (see supplementary materials) and XAS studies.

Fig. 6 shows the H_2-TPR results of 5 wt.% Mn/AC sample treated at different temperatures. For the 5 wt.% Mn/AC sample treated at 573 K and 673 K, they both show two broad reduction peaks at 723 K and 873 K, which suggests the similar oxidation states and dispersion of Mn species in these two samples. High pretreatment temperature (e.g., 873 K) significantly changes the H_2-TPR characteristics of Mn species on activated carbon. The areas of both reduction peaks decrease remarkably, and the onset reduction temperature of manganese oxide species as well as the second reduction peak shifts to a high temperature. As carbon can act a reductor, this increase in the pretreatment temperature can modify the strength of the bond between carbon and manganese, some reduction of manganese may also occur, leading to a remarkable change of onset reduction in the H_2-TPR characteristics. The decrease in reduction peak area may be related to the reduction of Mn^{3+} to Mn^{2+} by carbon under high temperature.

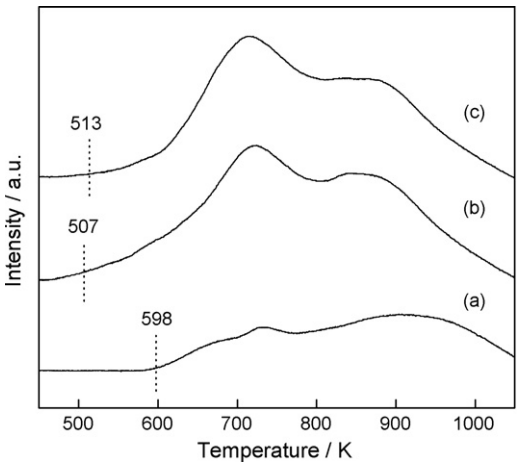

Fig. 6. H_2-TPR spectra for 5 wt.% Mn/AC samples under different treatment temperature: (a) 573 K; (b) 673 K; (c) 873 K.

3.5. Catalytic results

The manganese supported on activated carbon catalysts have been examined for the aerobic oxidation of benzyl alcohol using molecular O_2 as oxidant. As shown in Table 3, the Mn/AC catalysts prepared in this study can effectively catalyze the conversion of benzyl alcohol under mild conditions. The benzyl alcohol conversion increases with Mn loading, it reaches a maximum at the Mn content of ca. 10 wt.%. Further increase the Mn loading, however, does not increase the alcohol conversion significantly. As suggested by XRD and EXAFS, the manganese species with Mn loadings lower than 5 wt.% possess smaller particle size compared to that of 10 wt.% Mn/AC and 20 wt.% Mn/AC, the higher activities of 10 wt.% Mn/AC and 20 wt.% Mn/AC catalysts may be due to large number of surface sites. Therefore, the activity depends on two factors in this catalytic system: one is the smaller cluster size and the other factor is more surface active sites. The turnover number remains almost constant with Mn loadings below ca. 5 wt.%; further increasing Mn content leads to a remarkable decrease of turnover number. Based on XRD, XPS (see supplementary materials), EXAFS, and H_2-TPR characterizations, Mn species are highly dispersed on activated carbon surface with Mn loadings lower than ca. 5 wt.%, a higher Mn content results in large aggregated MnO_x particles, which shows poor catalytic efficiency evidenced by low turnover number. Therefore, highly dis-

Table 3
Effect of Mn content on catalytic properties of the Mn/AC samples treated at 673 K in the oxidation of benzyl alcohol with O_2.

Samples	Mn content/%	BET/$m^2\ g^{-1}$	Conv./%	Select./%	TON
AC	0	856	0.6	>99	–
1 wt.% Mn/AC	1.0	918	6.5	>99	3.5
2 wt.% Mn/AC	2.0	850	12.6	>99	3.4
3 wt% Mn/AC	3.0	798	19.2	>99	3.5
4 wt.% Mn/AC	4.0	773	25.4	>99	3.5
5 wt.% Mn/AC	5.0	758	30.6	>99	3.4
7 wt.% Mn/AC	7.0	727	34.8	>99	2.7
10 wt.% Mn/AC	10.0	694	42.5	>99	2.3
20 wt.% Mn/AC	20.0	633	42.3	>99	1.2

Conditions: catalyst = 0.2 g, benzyl alcohol = 2 mmol, T = 373 K, O_2 flow rate = 12 ml min^{-1}, t = 4 h.

Table 4
Effect of the treatment temperature on the catalytic performance of the 5 wt.% Mn/AC sample.[a].

Sample	Temperature/K	BET/$m^2\ g^{-1}$	Conv./%	Select./%
Mn/AC-473	473	764	25.0	>99
Mn/AC-573	573	745	27.1	>99
Mn/AC-673	673	758	30.6	>99
Mn/AC-773	773	768	29.3	>99
Mn/AC-873	873	826	20.1	>99
Mn/AC-973	973	881	7.2	>99

[a] Conditions: catalyst = 0.2 g, benzyl alcohol = 2 mmol, T = 373 K, O_2 flow rate = 12 ml min^{-1}, t = 4 h.

persed Mn species on activated carbon surface is suggested to be more catalytically active in the aerobic oxidation of benzyl alcohol using molecular O_2.

The pretreatment temperature shows significant effect on the catalytic performance (see in Table 4). The sample treated at 473 K exhibits a benzyl alcohol conversion of ca. 25.0%. Such a low conversion may be arouse from the partial decomposition of $Mn(NO_3)_2$ at this temperature. There is a slight increase of the benzyl alcohol conversion with increasing the treated temperature; the conversion reaches the maximum at 673 K pretreatment; further increase the temperature lowers the alcohol conversion. Although a high temperature can increase the surface area of the Mn/AC catalyst, a notable decrease of catalytic activity is observed as the pretreatment temperature is higher than 873 K. We also found that the actual Mn content over activated carbon is slight higher than 5 wt.% in this high-temperature treated sample. This suggests that carbon loss may occur during the treatment due to the oxidation of carbon. Although H_2-TPR, XAS, and ESR results suggest a significant change in the nature of Mn species in this particular high temperature treated samples, the reason why the activity decreases remains unclear up to now. One possible explanation is that more Mn^{2+} ions were formed due to the reduction of Mn^{3+} in the octahedral coordination assisted by carbon under high temperature.

4. Conclusions

The activated carbon supported manganese oxide catalysts have been prepared by a conventional wet impregnation method. Various characterizations suggested that this method mainly results in a highly dispersed Mn_3O_4 homogeneously distributed on the activated carbon surface, whereas more Mn ions located in tetrahedral coordination sites were observed compared to bulk Mn_3O_4. Aggregated MnO_x crystalline (mixture of Mn_3O_4 and MnO) would be formed with high Mn loadings. These highly dispersed manganese species, coexistence of Mn^{2+} and Mn^{3+}, were postulated to be the active sites in aerobic oxidation of benzyl alcohol with molecular O_2. The pretreatment temperature of catalyst had crucial effect on the nature of supported manganese oxide species. A high pretreatment temperature may lead to the reduction from Mn^{3+} to Mn^{2+} because of the carbon support as suggested by XANES and H_2-TPR, resulting in lower catalytic activity in the aerobic oxidation of benzyl alcohol.

Acknowledgments

This work was mainly supported by AcRF grant tier 2 ARC 13/07. We also thank to the National Natural Science Foundation of China (No. 20673034) and the Science Research Foundation for Young Skeleton Teachers working in the Universities of Henan Province of China. Work partially performed at SSLS under NUS Core Support C-380-003-003-001, A*STAR/MOE RP 3979908M and A*STAR 12 105 0038 grants.

Appendix A. Supplementary data

Supplementary data associated with this article can be found, in the online version, at doi:10.1016/j.molcata.2008.11.003.

References

[1] R. Radhakrishnan, S.T. Oyama, J.G. Chen, K. Asakura, J. Phys. Chem. B 105 (2001) 4245–4253.
[2] A. Nishino, Catal. Today 10 (1991) 107–118.
[3] M. Lo Jacono, M. Schiavello, in: B. Delmon, P.A. Jacobs, G. Poncelet (Eds.), Preparation of Catalysts I, vol. 1, Elsevier, Amsterdam, 1976, pp. 473–501.
[4] T. Yamashita, A. Vannice, J. Catal. 161 (1991) 254–262.
[5] J. Ma, G.K. Chuah, S. Jaenicke, R. Gopalakrishnan, K.L. Tan, Ber. Bunsen-Ges. Phys. Chem. 100 (1996) 585–593.
[6] S.B. Kanungo, J. Catal. 58 (1979) 419–435.
[7] G.K. Boreskov, in: J.R. Anderson, M. Boudart (Eds.), Catalysis Science and Technology, Springer-Verlag, Berlin, 1983, pp. 83–96.
[8] A. Maltha, T.L.F. Favre, H.F. Kist, A.P. Zuur, V. Ponec, J. Catal. 149 (1994) 364–374.
[9] M.A. Baltanas, A.B. Stiles, J.R. Katzer, Appl. Catal. 28 (1986) 13–33.
[10] W. Li, S.T. Oyama, in: B.K. Warren, S.T. Oyama (Eds.), Heterogenerous Hydrocarbon Oxidation, ACS Symposium Series, vol. 638, American Chemical Society, Washington, DC, 1996, pp. 364–372.
[11] Y.-C. Son, V.D. Makwana, A.R. Howell, S.L. Suib, Angew. Chem. Int. Ed. 40 (2001) 4280–4283.
[12] V.R. Choudhary, P.A. Chaudhari, V.S. Narkhede, Catal. Commun. 4 (2003) 171–175.
[13] Y. Su, L.-C. Wang, Y.-M. Liu, Y. Cao, H.-Y. He, K.-N. Fan, Catal. Commun. 8 (2007) 2181–2185.
[14] B. Dmuchovsky, M.C. Freerks, F.B. Zienty, J. Catal. 4 (1965) 577–580.
[15] A. Naydenov, D. Mehandjiev, Appl. Catal. A 97 (1993) 17–22.
[16] L. Singoredjo, R. Korver, F. Kapteijn, J. Moulijn, Appl. Catal. B 1 (1992) 297–316.
[17] G.K. Boreskov, Adv. Catal. 15 (1964) 285–339.
[18] J.P. Wakker, A.W. Gerritsen, J.A. Moulijn, Ind. Eng. Chem. Res. 32 (1993) 139–149.
[19] T. Valdés-Solís, G. Marbán, A.B. Fuertes, Catal. Today 69 (2001) 259–264.
[20] F. Kapteijn, A.D. van Langeveld, J.A. Moulijn, A. Andreini, M.A. Vuurman, A.M. Turek, J.M. Jehng, I.E. Wachs, J. Catal. 150 (1994) 94–104.
[21] T. Valdés-Solís, G. Marbán, A.B. Fuertes, Appl. Catal. B 46 (2003) 261–271.
[22] G. Marbán, T. Valdés-Solís, A.B. Fuertes, J. Catal. 226 (2004) 138–155.
[23] L.M. Gandía, M.A. Vicente, A. Gil, Appl. Catal. B 38 (2002) 295–307.
[24] J.C. Duchet, E.M. van Oers, V.H.J. de Beer, R. Prins, J. Catal. 80 (1983) 386–402.
[25] Z.-R. Li, Y.-L. Fu, M. Jiang, T.-D. Hu, T. Liu, Y.-N. Xie, J. Catal. 199 (2001) 155–161.
[26] R. Moene, F.W. Tazelaar, M. Makkee, J.A. Moulijn, J. Catal. 170 (1997) 311–324.
[27] T. Grzybek, J. Klinik, M. Rogóz, H. Papp, J. Chem. Soc., Faraday Trans. 94 (1998) 2843–2850.
[28] A. Nishijima, Y. Kiyozumi, A. Ueno, M. Kurita, H. Hagiwara, S. Toshio, N. Todo, Bull. Chem. Soc. Jpn. 52 (1979) 3724–3727.
[29] J. Ogonowski, E. Skrzyńska, Catal. Lett. 111 (2006) 79–85.
[30] X. Tang, J. Hao, H. Yi, J. Li, Catal. Today 126 (2007) 406–411.
[31] S. Vankova, T. tsoncheva, D. Mehandjiev, Catal. Commun. 5 (2004) 95–99.
[32] M. Ouzzine, G.A. Cifredo, J.M. Gatica, S. Harti, T. Chafik, H. Vidal, Appl. Catal. A 342 (2008) 150–158.
[33] M. Yoshikawa, A. Yasutake, I. Mochida, Appl. Catal. A 173 (1998) 239–245.
[34] G. Marban, A.B. Fuertes, Appl. Catal. B 34 (2001) 43–53.
[35] G. Marban, A.B. Fuertes, Appl. Catal. B 34 (2001) 55–71.
[36] H.O. Moser, B.D.F. Casse, E.P. Chew, M. Cholewa, C.Z. Diao, S.X.D. Ding, J.R. Kong, Z.W. Li, M. Hua, M.L. Ng, B.T. Saw, S. bin Mahmood, S.V. Vidyaraj, O. Wilhelmi, J. Wong, P. Yang, X.J. Yu, X.Y. Gao, A.T.S. Wee, W.S. Sim, D. Lu, R.B. Faltermeier, Nucl. Instr. Methods Phys. Res., Sect. B 238 (2005) 83–86.
[37] S.I. Zabinsky, J.J. Rehr, A. Ankudinov, R.C. Albers, M.J. Eller, Phys. Rev. B 52 (1995) 2995–3009.
[38] W.S. Kijlstra, E.K. Poels, A. Bliek, B.M. Weckhuysen, R.A. Schoonheydt, J. Phys. Chem. B 101 (1997) 309–316.
[39] J.C. Védrine, in: F. Delanny (Ed.), Characterization of Heterogeneous Catalyst, Marcel Dekker, New York, 1984, pp. 161–176.
[40] S. Velu, N. Shah, T.M. Jyothi, S. Sivasanker, Microporous Mesoporous Mater. 33 (1999) 61–75.
[41] Q. Zhang, Y. Wang, S. Itsuki, T. Shishido, K. Takehira, J. Mol. Catal. A 188 (2002) 189–200.
[42] G. Brouet, X. Chen, C.W. Lee, L. Kevan, J. Am. Chem. Soc. 114 (1992) 3721–3726.
[43] E. Checheva, M. Gorova, R. Stoyanova, J. Mater. Chem. 9 (1999) 1559–1567.
[44] F.E. Huggins, N. Shah, G.P. Huffman, J.D. Robertson, Fuel Process. Technol. 65–66 (2000) 203–218.
[45] J. Qi, M. Zhang, L. Feng, X. Li, Z. Xie, Z. Sun, T. Hu, Molecules 8 (2003) 31–39.
[46] S. Priggemeyer, P. Eggers-Borkenstein, F. Ahlers, G. Henkel, M. Körner, H. Witzel, H.F. Nolting, C. Hermes, B. Krebs, Inorg. Chem. 34 (1995) 1445–1454.
[47] Y. Kou, B. Zhang, J. Niu, S. Li, H. Wang, T. Tanaka, S. Yoshida, J. Catal. 173 (1998) 399–408.

[48] N.M.D. Brown, J.B. Mcmonagle, G.N. Greaves, J. Chem. Soc., Faraday Trans. 1 (80) (1984) 589–597.
[49] R. Radhakrishnan, S.T. Oyama, Y. Ohminami, K. Asakura, J. Phys. Chem. B 105 (2001) 9067–9070.
[50] C. Reed, Y.K. Lee, S.T. Oyama, J. Phys. Chem. B 110 (2006) 4207–4216.
[51] Y. Yang, R. Huang, L. Chen, J. Zhang, Appl. Catal. A 101 (1993) 233–252.
[52] Y. Han, F. Chen, K. Ramesh, Z. Zhong, E. Widjaja, L. Chen, Appl. Catal. B 76 (2007) 227–234.
[53] V. Baron, J. Gutzmer, H. Rundlöf, R. Tellgren, Am. Miner. 83 (1998) 786–793.
[54] J. Laine, A. Calafat, M. Labady, Carbon 27 (1989) 191–195.
[55] J. Laine, F. Severino, M. Labady, J. Catal. 147 (1994) 355–357.
[56] A. Calafat, J. Laine, A. López-Agudo, J.M. Palacios, J. Catal. 162 (1996) 20–30.